Morphological Development of Impact Polypropylene Produced in Gas Phase with a $TiCl_4/MgCl_2$ Catalyst

JON A. DEBLING,[1] W. HARMON RAY[2]

[1] Johnson Polymer, 8310 16th Street, P.O. Box 902, Sturtevant, Wisconsin 53177-0902

[2] Department of Chemical Engineering, University of Wisconsin-Madison, Madison, Wisconsin 53706-1691

Received 20 September 1999; accepted 7 November 1999

ABSTRACT: This article reports on a comprehensive study of the reaction kinetics, particle morphology development, and polymer properties of impact polypropylene produced in gas phase with a $TiCl_4/MgCl_2$ catalyst. Experiments were conducted over a range of copolymerization times, temperatures, monomer compositions, and hydrogen levels. The catalyst was found to exhibit a decay-type reaction rate for ethylene and propylene, but the presence of both monomers together caused an activation of the catalyst. Copolymer composition was constant over reaction time. Hydrogen was found to reversibly enhance the rate of propylene polymerization but to have no effect on ethylene. Microscopy provided evidence that the copolymer phase segregates from the homopolymer during polymerization. As copolymer content increased, product bulk density decreased because of the presence of sticky material on the particle surface. However, even at 70 wt % copolymer, enough pores were present in the particle to prevent monomer diffusion limitations. © 2001 John Wiley & Sons, Inc. J Appl Polym Sci 81: 3085–3106, 2001

Key words: impact polypropylene; morphology; Ziegler–Natta; diffusion; gas phase; SEM; scanning FTIR; composition gradients

INTRODUCTION

Impact polypropylene is an important commercial polyolefin produced by solid catalyzed olefin polymerization in a multistage process consisting of a train of reactors in a series. In the first stage of the process isotactic polypropylene is produced, and in the second stage an ethylene propylene copolymer is added to the previously formed homopolymer. Typical catalysts include high-activity-supported $TiCl_4/MgCl_2$ Ziegler–Natta, unsupported $TiCl_3$, and recently commercialized Metallocene systems. Thus, from each catalyst particle fed to the beginning of the reactor train, a single polymer granule develops and is collected at the end of the process.

Numerous researchers have studied the polymerization kinetics[1–5] and morphological development[2,6–15] of polypropylene produced with solid catalysts. A number of kinetic models have been proposed, and there is still much debate about the mechanisms involved and number of catalyst site types active for polymerization. There is, however, a fair amount of agreement that the morphology of the polypropylene particle tends to replicate that of the original catalyst. Isotactic polypropylene granules are generally porous and consist of firmly bound small polymeric structures called "microparticles," each of which contains a fragment of catalyst inside. The product usually has high bulk density.

Correspondence to: W. H. Ray (ray@engr.wisc.edu).

Journal of Applied Polymer Science, Vol. 81, 3085–3106 (2001)

Only a few studies on impact polypropylene kinetics or morphology have been reported in the published literature. Kakugo et al.[16,17] investigated the morphology of impact polypropylene produced under liquid pool–gas conditions with a Mg–Ti catalyst. Although the polypropylene homopolymer was found to be porous and contained well-defined microparticles, TEM micrographs of sectioned and stained impact copolymer particles over a large range of copolymer contents indicated the copolymer phase had relocated to the interstices of the homopolymer matrix. At high copolymer content essentially nonporous particles were found. Simonazzi et al.[18] reported that when the copolymer phase is added to the homopolymer particle, it intimately dispersed within the preexisting voids. Montell terms these particles "heterophasic" to indicate the phase segregation of the copolymer and homopolymer phases from each other.[8,18,19] Galli has written numerous informative articles on the design of industrial high-activity $TiCl_4/MgCl_2$ catalysts for the controlled morphology of impact polypropylene, including reporting on the most recent advances.[19]

The unique structures reported for impact polypropylene suggest that morphology may play an important role in the polymerization process. The potential for monomer mass transfer limitations exists when particle porosity becomes low, as has been found by others in ethylene–propylene random copolymerization.[1,20] The presence of segregated copolymer has also been suggested as a reason for particle sticking in the reactor environment.[18]

In this article a study of the reaction kinetics, particle morphology development, and polymer properties of impact polypropylene produced in gas phase is reported. To date, this is the first comprehensive study of its kind published in the open literature.

EXPERIMENTAL

All experiments were conducted in gas phase with a 1-l Parr reactor operated horizontally. A complete description of the design and flexibility of the reactor system is presented in Debling.[21] Figure 1 shows a schematic of the reactor system.

Experiments were performed with a high-activity $TiCl_4/MgCl_2$ catalyst with triethylaluminum (TEA) as cocatalyst and cyclohexyl-methyldimethoxysilane (CHMMS, Aldrich Chemicals, Milwaukee, WI) as external donor. Storage and preparation of catalyst materials was conducted in an inert glovebox atmosphere. The external donor was first contacted with the cocatalyst for 5 min at an Al–Si molar ratio of 10 : 1 to provide complexation. Dry catalyst (50 mg) was then contacted with the mixture and 2 cm^3 of heptane in a section of $\frac{3}{8}''$ stainless tubing with two-way valves at each end for 10 min at an Al–Ti molar ratio of 30 : 1. Attached to this device was a section of $\frac{1}{2}''$ tubing and a three-way valve containing 5 mL of a hexane wash.

The reactor was first charged with 160 g of Teflon™ powder (DuPont, Wilmington, DE), granular resin 9B seed bed, then purified for 2 h under vacuum at 70°C, followed by repeated nitrogen flushes to remove air and moisture. After heat evacuation was complete, the reactor was cooled to 40°C and the catalyst charged to the reactor using nitrogen pressure to force the slurry mixture into the system. Timing was set so this was done after precisely 10 min of contact time of the Al–Ti. Heptane and hexane were removed by repeated flushes with cold nitrogen and nitrogen removed by three flushings with propylene. The set point of the reactor temperature was then adjusted to reaction conditions. During these initial steps prepolymerization of the catalyst was done at a low temperature to avoid particle fragmentation.

All gases used were first purified on-line by passing over a three-stage purification train consisting of oxygen scavenger (BASF R3-11 for ethylene and propylene, Fisher RIDOX for nitrogen and hydrogen), molecular sieves, and activated alumina. The individual gases were then filtered (7 μm), and the flow of each gas was independently measured and controlled with a Teledyne Hastings mass flow controller. Reactor temperature was controlled with a PI controller that manipulated the flow of cooling water through cooling coils soldered to the outside of the reactor. An electrical heating jacket surrounding the reactor was in the "on" position for most of the experimental run. Constant reactor pressure was maintained with a back-pressure regulator and a continuous reactor purge.

Gas phase composition was determined on-line with a Galaxy 3020 FTIR from ATI/Mattson instruments. The reactor purge gas was fed to a temperature-controlled 5-cm beam-conforming gas cell with KBr lenses and a cell volume of 10 cm^3. Propylene composition in ethylene–propylene–hydrogen–nitrogen mixtures was determined by inspection of the absorbence at wavelengths in the 473.51–678.42 range. Typically four scans of weighted sample were used, for a total cycle time of 15 s for the analysis. The composition of the gas

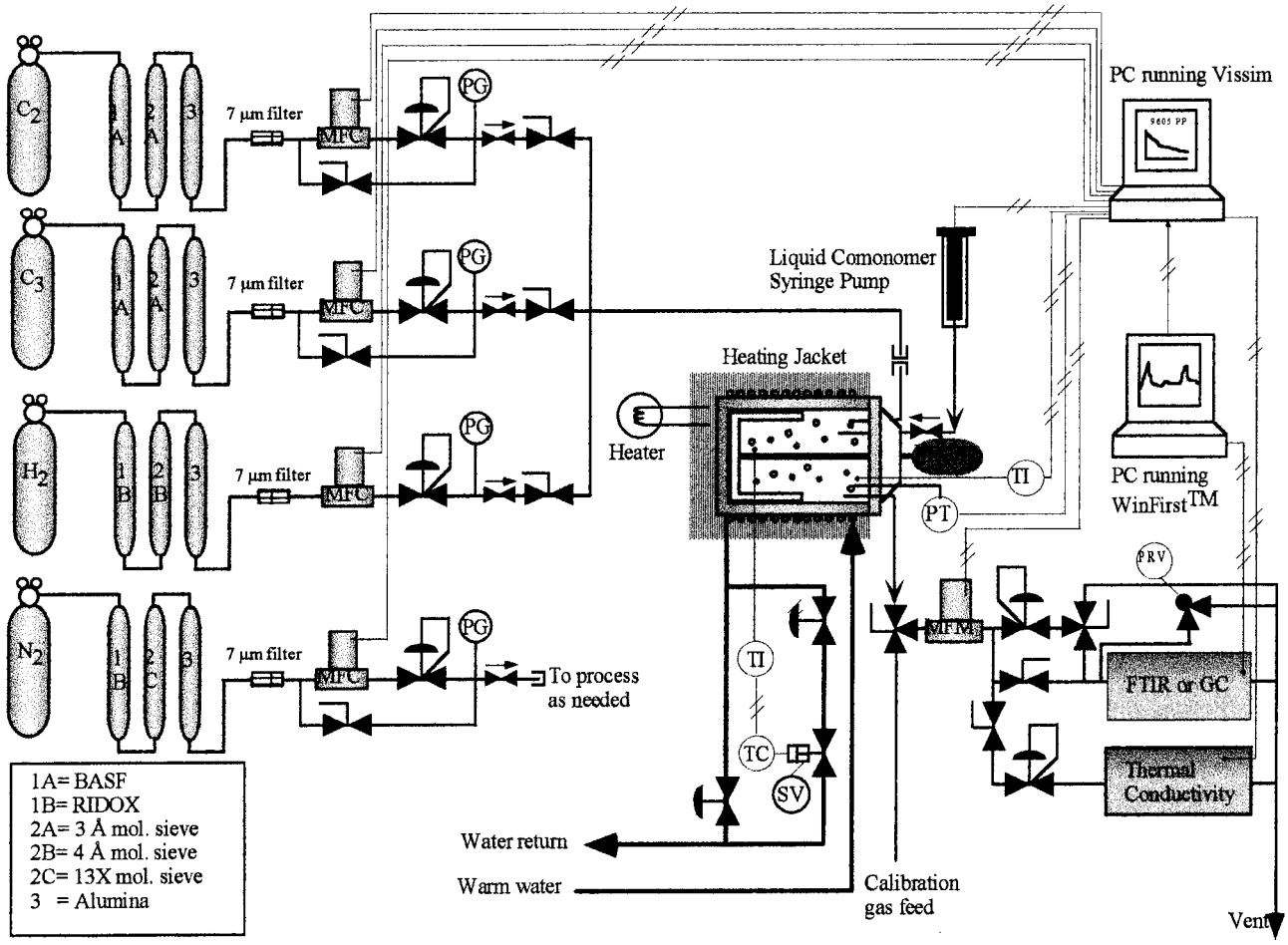

Figure 1 Horizontal stirred-bed gas phase reactor system.

was calculated from linear models obtained from calibration gas mixtures and communicated to the digital-to-analog board of the computer using WINFIRST™ IR software (Middleton, WI). A separate computer monitored the process data and controlled the reactor, using the data-acquisition package VISSIM™ (Westford, MA). Composition was controlled by PID control loops manipulating the feed composition, and the hydrogen level was set by a model-based control scheme. At the end of the experiment the polymer product was separated from the Teflon™ in water and soap, air-dried, and treated with antioxidant. Rates of reaction of each monomer were calculated by reactor mass balance and scaled by the total amount of titanium in the catalyst and by the monomer concentration sorbed into the polymer.[2] Thus, rates are expressed in L, amorphous polymer/mole total titanium/unit time. In examples where comparisons of different runs are made, the absolute rates were scaled to account for run-to-run variances so that the homopolymerization rate curves overlapped.

Scanning electron microscopy was conducted with a Hitachi S800 6KV machine. Sectioned samples were first embedded in EPON™ 812 resin, then sectioned with a diamond knife in a Riechert-Jung FC4E cryogenic ultramicrotome operating at −60°C. TEM slices were analyzed with a Hitachi H8-100 machine at 150 KV. GPC results were obtained with Mark Houwink coefficients of $k = 8.33 \times 10^{-5}$ and $a = 0.8$. DSC samples were first equilibrated at 25°C, then ramped at a rate of 50°C/min to 230°C, and then held isothermal for 10 min. The sample was then cooled to 48°C at a rate of 10°C/min. After cooling, the polymer was increased to 210°C at a rate of 10°C/min.

RESULTS

Catalyst Polymerization Behavior

Rate vs. Time Profiles

Ethylene and propylene homopolymerization behaviors are characterized by an initial high activ-

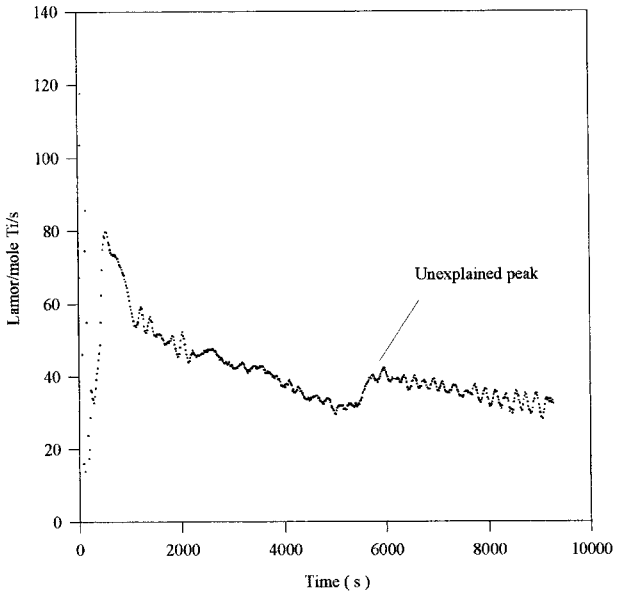

Figure 2 Typical homopolymerization behavior of ethylene: 60°C, 3.1 atm, 5 mol % H_2.

ity and rapid decay, followed by a more stable but still decaying profile [Figs. 2 and 3(a)]. The profiles are not well described by a first-order exponential decay model. The catalyst was found to be immediately active for (or to be rapidly activated by) both monomers. Although the catalyst continues to decay during propylene homopolymerization, a distinct unexplained rise in activity well into the experiment was observed for ethylene homopolymerization. This behavior has been observed by others with similar catalysts during ethylene (co)polymerization without the use of external donors.[22,23]

Figure 3 illustrates the typical catalyst behavior found for impact polypropylene experiments. Upon addition of ethylene to the reactor, the rate of polymerization of both monomers increases slowly (well after gas phase composition transients have been completed) to a peak value, then begins to decline. Instantaneous copolymer composition remains relatively constant during the entire copolymerization stage of the experiment, even for products containing up to 70 wt % copolymer.

Further experimentation showed the observed peak in activity during ethylene–propylene copolymerization to be temperature dependent (Fig. 4). As copolymerization temperature increased, the peak appeared earlier. The appearance of the peak was apparently not affected by the length of the homopolymerization stage (Fig. 5) as it could be reproduced in experiments involving 3 h of propylene homopolymerization. Furthermore, the presence of both ethylene and propylene simultaneously was found to be necessary for the "activation" effect to occur. Figure 6 shows experiment

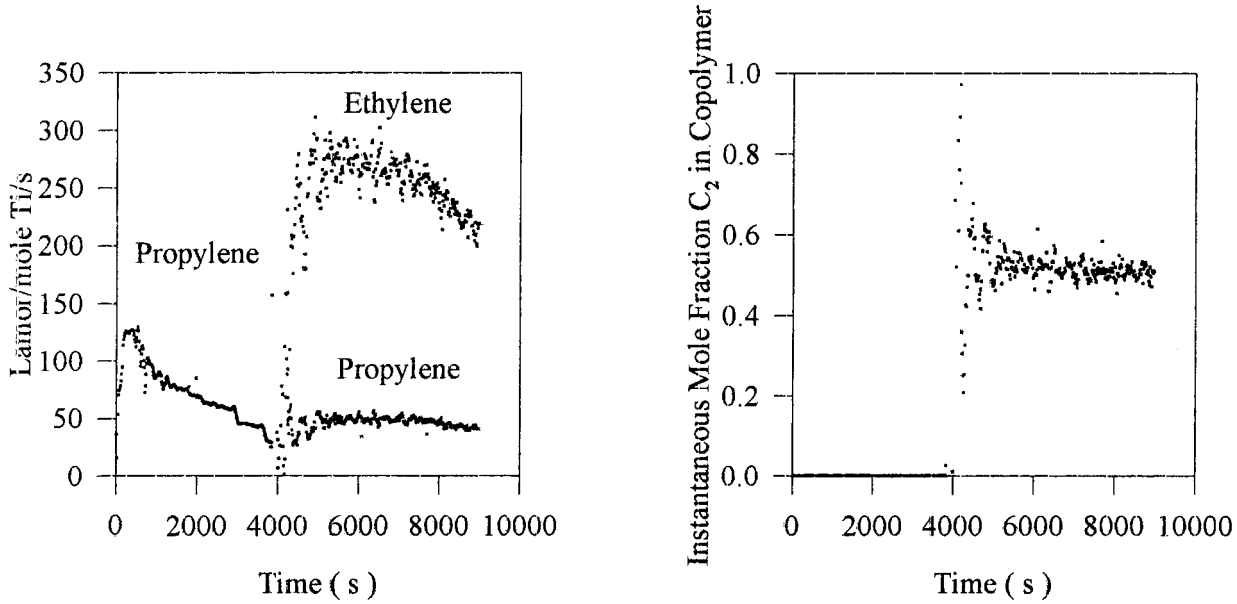

Figure 3 Typical catalyst behavior for impact polypropylene production at (a) rate versus time and (b) instantaneous composition: C_3 stage at 70°C, 3.1 atm, 5 mol % H_2, duration of 1 h; C_2/C_3 stage at 60°C, 3.1 atm, 5 mol % H_2.

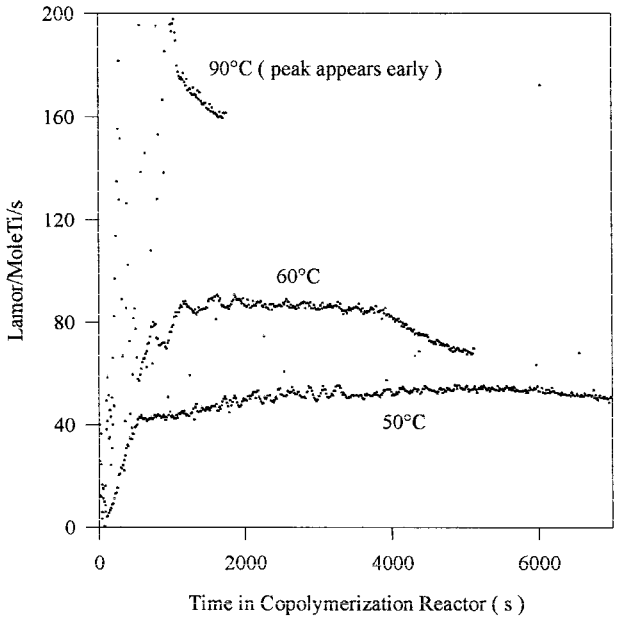

Figure 4 Effect of temperature on catalyst activation during copolymerization: C_3 stage at 70°C, 3.1 atm, 5 mol % H_2, duration of 1 h; C_2/C_3 stage at 1.7 atm, 5 mol % H_2.

where the catalyst was polymerized first with propylene, followed by ethylene (after flushing the system 20 times with pure N_2 and 10 additional times with pure ethylene to remove residual propylene). The decay-type behavior of the catalyst in the presence of only ethylene monomer is evident. However, when propylene is added back to the system after a 2.5-h polymerization time, a slow activation of the catalyst was observed. The activity of the catalyst (both ethylene and propylene rate) continues to rise for almost 1.5 h and approaches 150% of the initial copolymerization activity. A pronounced peak and subsequent decay in activity was then observed. During this experiment the instantaneous polymer composition remained constant at approximately 50 mol % ethylene.

Reactivity Ratios

Reactivity ratios at 60°C were determined from experiments involving stepwise changes in gas composition (all other factors constant). Both steps up and down in composition were performed in separate experiments. Data were collected after the peak in activity previously described had subsided. "Apparent" reactivity ratios of $r_1 = 0.132$ and $r_2 = 4.91$ and (propylene = 1, ethylene = 2) were calculated using the Fineman and Ross technique (Figure 7).

After the peak in activity had passed, reducing the propylene mole fraction in the gas phase always led to increased reaction rates for both monomers (Fig. 8), which is expected from the copolymerization kinetics.

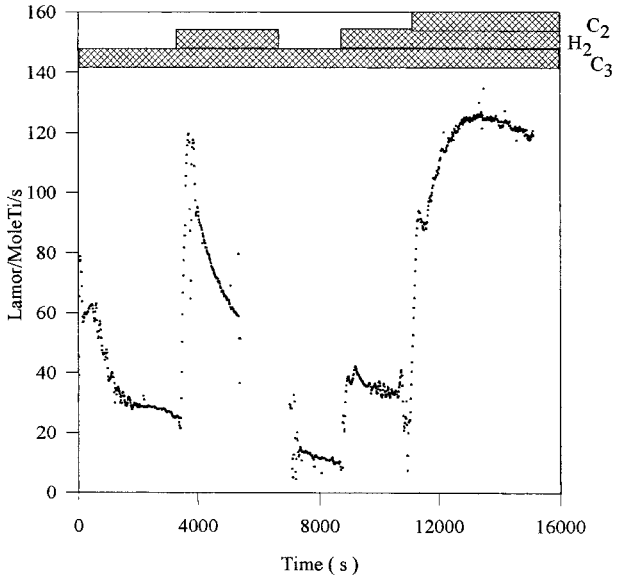

Figure 5 Effect of homopolymerization time on catalyst activation: C_3 stage at 70°C, 3.1 atm, 5 mol % H_2, duration of 3 h; C_2/C_3 stage at 1.7 atm, 5 mol % H_2.

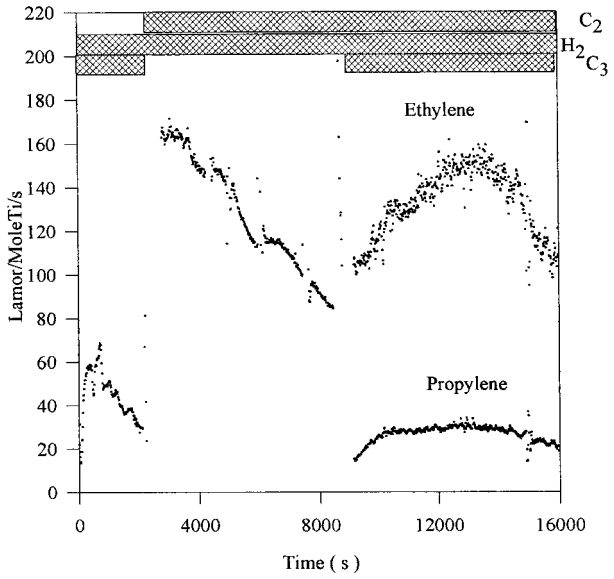

Figure 6 Effect of feed sequencing on catalyst activation: C_3 stage at 70°C, 3.1 atm, 5 mol % H_2, duration of 3 h; C_2 and C_2/C_3 stage at 60°C, 1.7–4.7 atm, 5 mol % H_2.

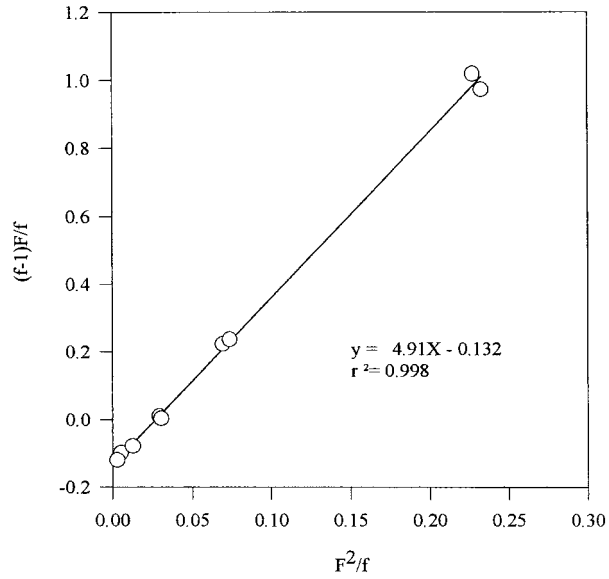

Figure 7 Reactivity ratios by the Fineman and Ross technique: 60°C, 3.1 atm, 5 mol % H_2.

Reaction Order and Polymerization Activation Energy

The rate dependency on monomer concentration was determined by making a series of step changes in total reactor pressure while maintaining hydrogen at 5 mol % in the gas phase and making suitable corrections for the number of sites that had deactivated during the transition. For both monomers, a reaction order of close to 1 was found during homopolymerization and copolymerization (Fig. 9). Hamba et al.[22,23] have reported orders of 1 for propylene and ethylene propylene copolymerization experiments but have indicated the reaction order for ethylene during homopolymerization is greater than 1. Slow catalyst activation by ethylene was concluded to be the most likely explanation for this effect. However, these earlier experiments did not utilize external donors nor was the catalyst prepolymerized with propylene.

Activation energies for monomer propagation and catalyst deactivation were determined up and down stepwise perturbations in a reactor temperature initiated 30 min into the polymerization experiment (Figure 10). For each temperature interval the reaction rate was estimated by an exponential decay model. Table I summarizes the results. In general, higher propagation activation energies are obtained when the experiment involved steps up in temperature. The differences between the two cases are similar for propylene and ethylene, most likely indicating occurrence of temperature activation of the catalyst. Activation energies for copolymerization are similar for both monomers. The activation energy for deactivation was also higher than that of propagation, indicating that increasing temperature

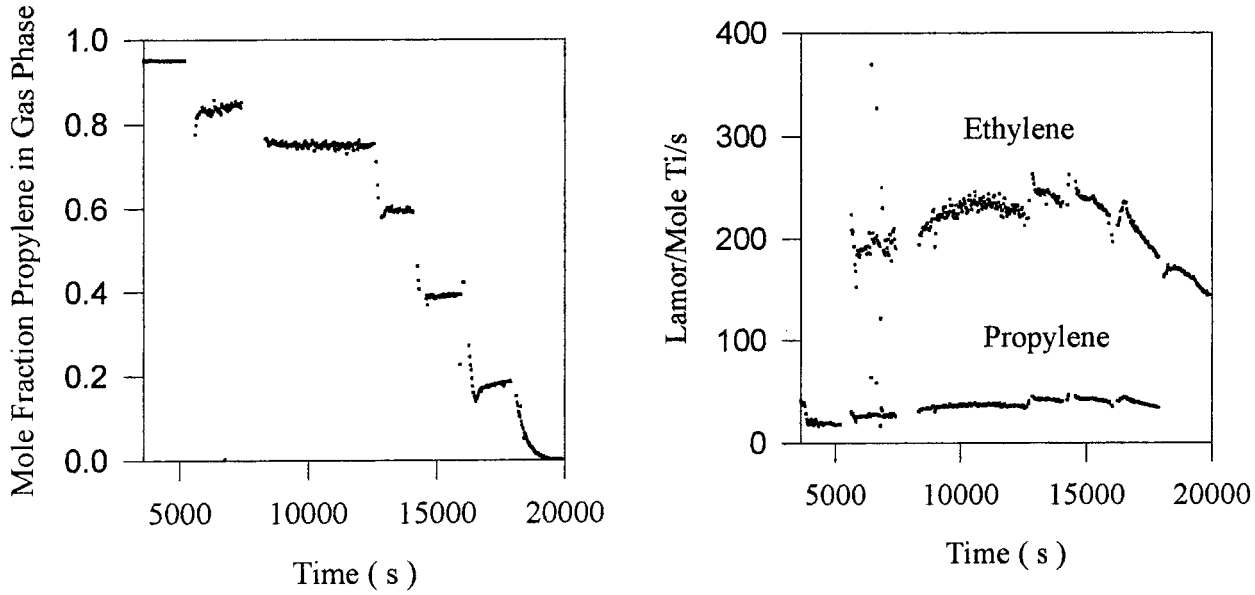

Figure 8 Effect of composition on reaction rate—(a) steps in composition, (b) rate versus time: C_3 prepolymerization stage at 70°C, 3.1 atm, 5 mol % H_2, C_2/C_3 copolymerization at 60°C, 3.1 atm, 5 mol % H_2.

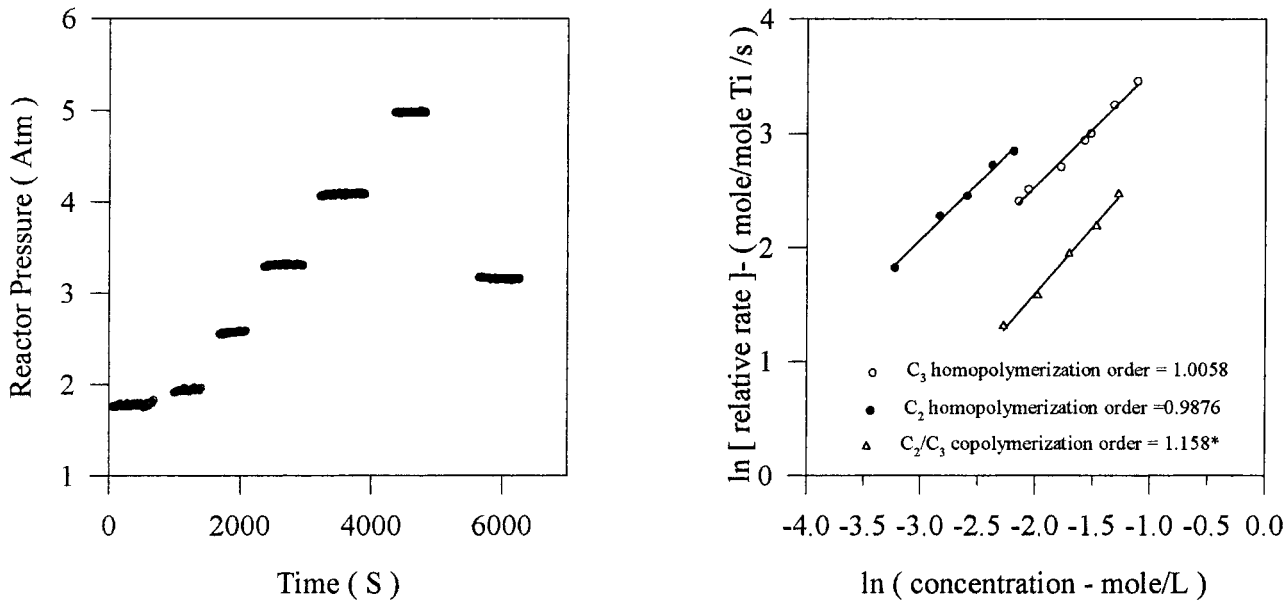

Figure 9 Determination of reaction rate dependency on monomer concentration—(a) reactor pressure steps and (b) rate versus concentration: All runs prepolymerized with C_3 at 70°C, 3.1 atm, 5 mol % H_2 for ~ 1 h; C_2 homopolymerization at 60°C, 5 mol % H_2; C_2/C_3 copolymerization at 60°C, 5 mol % H_2, 60 mol % C_3.

would not necessarily be the best way to increase catalyst productivity in a commercial process.

Effect of Hydrogen

The addition of hydrogen to the reactor can boost the rate of propylene polymerization by a factor of 3 at as low as 5 mol % in the gas phase and tends to increase the rate of catalyst deactivation [Fig. 11(a)]. The majority of the rate boost occurs at as little as 1 mol % hydrogen. This effect is also reversible, as noted by others.[24] Figure 11(b) shows an experiment where the catalyst was pre-

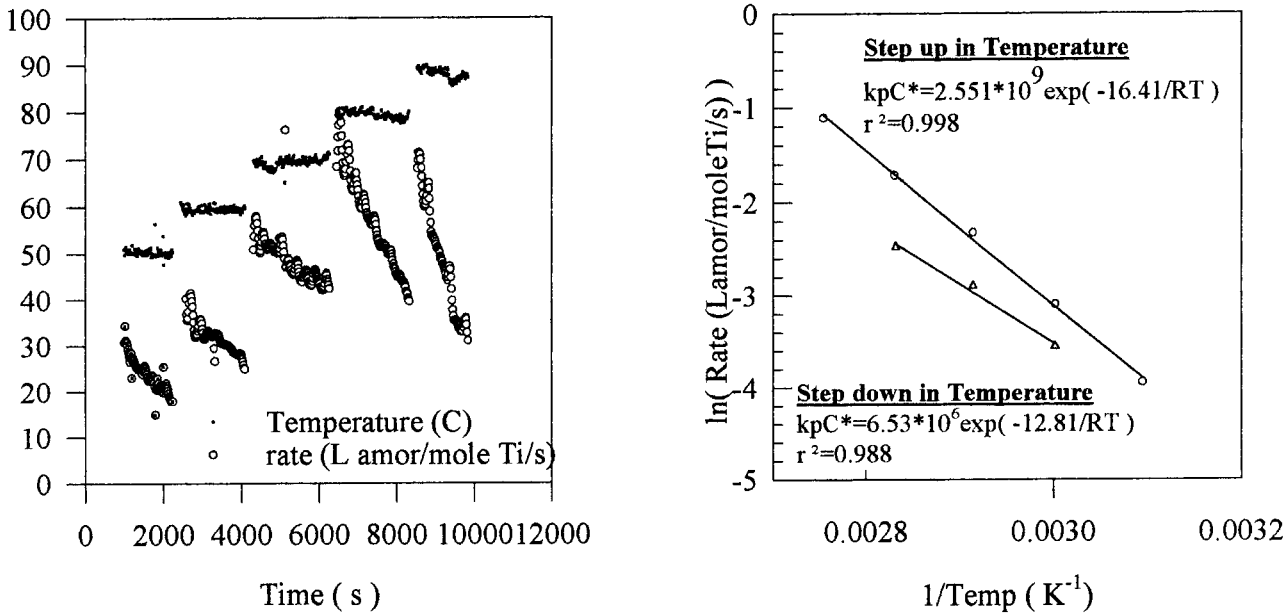

Figure 10 Calculation of activation energy of propylene homopolymerization—(a) example of temperature steps and rate response, (b) determination of activation energy; 3.1 atm, 5 mol % H_2.

Table I $TiCl_4/MgCl_2$ Catalyst Behavior Summary

	Homopolymerization		Copolymerization	
	Propylene	Ethylene	Propylene	Ethylene
Propagation[a]				
E_{act} for stepping up in temperature	16.41 Kcal/mol	13.3 Kcal/mol	9.9 Kcal/mol	9.19 Kcal/mol
E_{act} for stepping down in temperature	12.81 K cal/mol	7.7 K cal/mol	—	—
Deactivation[a]				
E_{act} for stepping up in temperature	19.45 Kcal/mol	18.68 Kcal/mol	18.47 Kcal/mol	19.39 Kcal/mol
Rate profile[a]	decay	decay with delayed peak	1) activation of catalyst when both monomers are present 2) presence of peak is temperature dependent 3) constant copolymer composition with time	
Effect of hydrogen				
effect on rate	reversible rate boost	none	small boost	none
effect on catalyst deactivation	increased deactivation	none	increased deactivation	increased deactivation
Measured reaction order[a]				
@ 70°C	1.006	—	—	—
@ 60°C		0.987		1.158
Reactivity ratios			$r_1 = 0.132$ and $r_2 = 4.91$	

[a] Experiments with 5 mol % hydrogen in gas phase.

polymerized with propylene as described earlier, the propylene was removed, and the reactor was flushed with nitrogen. Upon being fed ethylene, a decay-type rate was found. Hydrogen was then added to 5% of the gas phase at about 5000 s and to 10% at 7000 s reaction time. The data suggests hydrogen did not have any effect on the ethylene homopolymerization rate [Fig. 11(b)]. When hydrogen was removed at 8000 s, no change in ethylene rate was noticed. During copolymerization hydrogen only affected the rate of propylene homopolymerization.

Polymer Properties

A series of impact polypropylene samples was prepared under a variety of experimental conditions using the same level of Al–Ti and Al–Si ratios and catalyst preparation methods described earlier. A summary of the properties of the polymer is indicated in Table II.

As indicated by GPC analysis (Figure 12), the samples had a fairly low molecular weight and broad polydispersity under the hydrogen levels used in this work. At the same hydrogen level, the molecular weight of the impact copolymer resin was higher than that of the homopolymer, reflecting a higher molecular weight for the copolymer phase. This is because of the higher reactivity of ethylene and apparently similar rate of chain transfer to hydrogen that is the dominant method of chain termination. The molecular weight of the copolymer phase can be crudely estimated (without tedious extraction of the copolymer phase of impact polypropylene) from the molecular weights of homopolymer and impact copolymer samples produced in separate experiments under identical conditions:

$$Mw_{\text{total}} = \sum_{j=1}^{2} Mw_j \varphi_j \tag{1}$$

$$Mn_{\text{total}} = \left(\sum_{j=1}^{2} \frac{\varphi_j}{Mn_j} \right)^{-1} \tag{2}$$

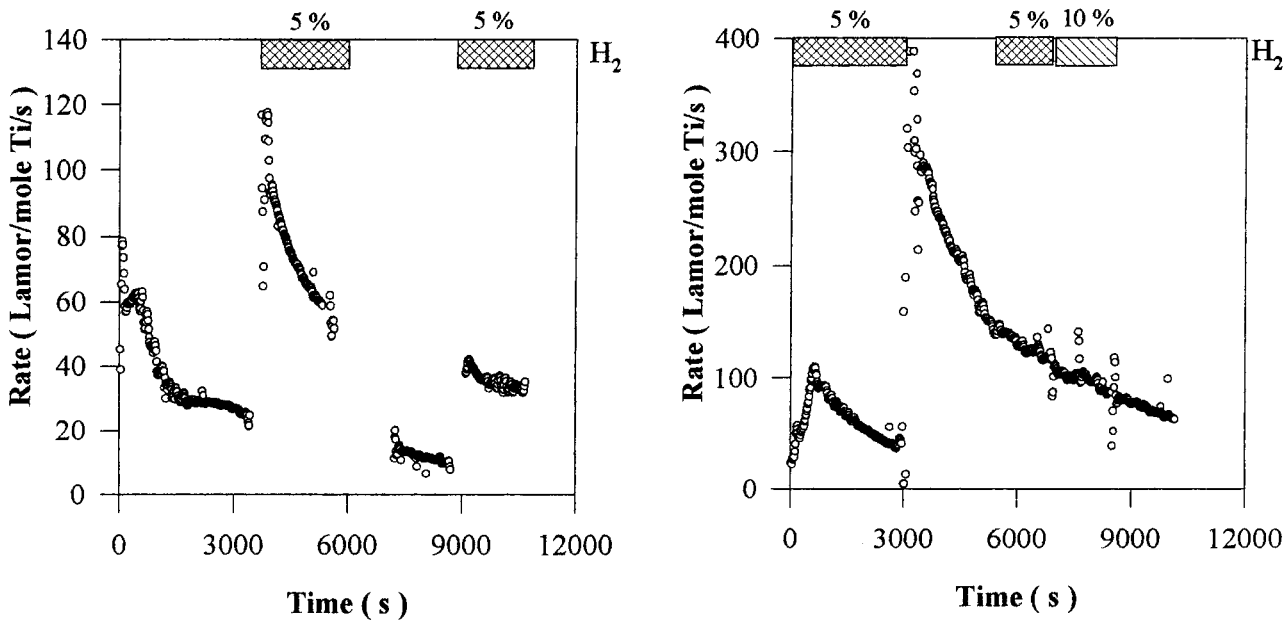

Figure 11 Effect of hydrogen on ethylene and propylene reaction rate—(a) propylene polymerization and (b) ethylene polymerization; C_3 stage at 70°C, 3.1 atm, 0–5 mol % H_2; C_2 stage at 60°C, 1.7 atm, 0–10 mol % H_2.

This assumes a physical blend of homopolymer and copolymer, with 1 designating the homopolymer phase and 2 the copolymer phase. Direct application of eqs. (1) and (2) from the data of Table II leads to a copolymer number-average molecular weight higher than the weight average because of the presence of a small peak at the low molecular weight range of the homopolymer sample that does not appear in the impact copolymer sample. The GPC molecular weights were then recalculated by removing this fraction from the distribution (these may be oligomeric chain lengths < 25 units, with impurities in the sample or choice of starting point for measuring elution volume), and the resulting "adjusted" molecular weights are shown in Table II.

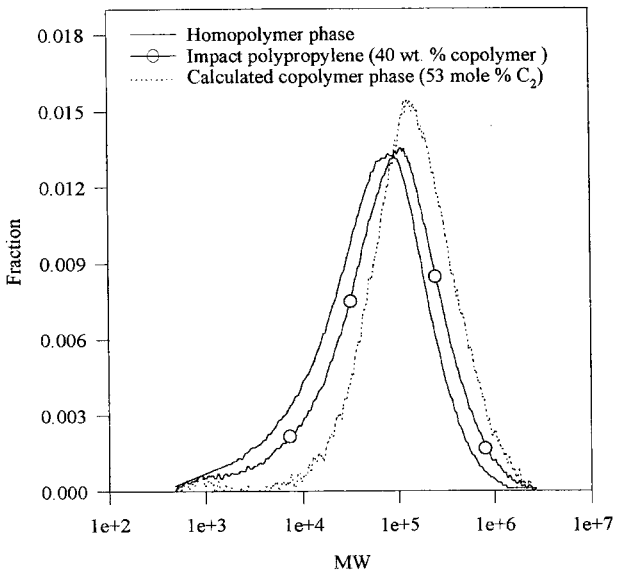

Figure 12 Molecular weight distribution of impact copolymer—adjusted GPC results.

Melt index of the impact polypropylene is shown as a function of operating conditions, copolymer content, and copolymer composition (Fig. 13). The trends show the expected results, that is, for a given hydrogen level in the reactor, increasing the copolymer fraction or ethylene content increases product molecular weight and therefore decreases melt index. Increasing copolymerization temperature produces a higher melt index product, from which it can be inferred that chain transfer to hydrogen reactions have a higher activation energy than propagation.

DSC analysis (Fig. 14) reveals a polypropylene melting point of 160°C and a crystallinity of 46%, based on the heat of fusion (95.35 J/g) and assuming 209 J/g for pure crystalline polypropylene.[25] The presence of a small endotherm in the DSC at 117°C is believed to be an ethylene-rich copolymer produced with a multisite Ziegler–Natta catalyst. The crystallinity of this fraction is esti-

Table II Reaction Conditions and Product Properties

	Copolymerization Stage Condition				Polymer Properties					Powder Properties		
Run	P (Atm)	T (°C)	C_a[a] (mol %)	H_2[a] (mol %)	Copolymer wt %[b]	Copolymer[b] (C_2 mol %)	Mn[c]	Mw[c]	MI[c]	ρ_{bulk} (g/cm^3)	Yield (g/g)	Dp Mean (μm)[e]
9654	—	—	—	—	—	—	—	—	—	0.509	972	769
9655	—	—	—	—	—	—	—	—	—	0.506	444	606
9662	—	—	—	—	—	—	—	—	—	0.471	1,380	812
9706	1.7	60	55	5	15.7	54.6	—	—	—	0.512	1,239	785
9707	1.7	60	58	5	40.4	53.0	28,532	157,117	21.28	0.459	1,622	1,107
9709	1.7	60	80	5	38.9	24.7	—	—	45.83	0.522	2,220	—
9712	—	—	—	5	—	—	17,532[c] 20,417[d]	107,645[c] 111,495[d]	124.4	—	784.7	—
9718	1.7	60	30	5	42.1	77.8	—	—	3.924	0.348	1,542	—
9720	3.1	60	60	5	70.3	52.8	—	—	2.77	0.314	2,136	885
9722	3.1	60	54	15	43.8	50.8	22,429	121,787	50.89	—	1,053	—
9723	3.1	90	60	5	42.5	48.5	—	—	36.49	0.458	966	—
9724	3.1	45	60	5	41.7	55.5	—	—	18.45	0.486	978	—
9738	3.1	60	60	5	70.0	54.6	—	—	—	0.414	2,460	923

Homopolymerization @ 70°C, 3 Atm, 5 mole % H_2 in gas phase unless otherwise noted.
[a] Mole % in gas phase.
[b] Calculated by mass balance.
[c] By GPC analysis.
[d] Adjusted GPC curve.
[e] Mechanical seiving.

mated to be only 1–2 wt %, assuming a heat of fusion of 154 J/g for crystalline LLDPE. No evidence of unusual composition broadening is indicated in DSC curves of up to 70 wt % copolymer. Furthermore, the DSC endotherms of three sizes of particles separated by mechanical sieving from the 70 wt % copolymer sample are similar. Significant composition broadening would be expected in the case of monomer diffusion limitations present during polymerization and would be more apparent in the larger particles.

Particle Morphology

SEM analysis of impact copolymer granules of up to 70 wt % copolymer are shown in Figure 15. Reaction conditions are indicated in Table II. It is noted that all the particles are very spherical in shape, suggesting the original shape of the homopolymer particle (and presumably the catalyst) is retained during the copolymerization stage, however; the texture of their surfaces differs. As the copolymer content increases, parts of the surface of the granule have the appearance of a smooth coating. The particles with more than 40 wt % copolymer have small chunks of material adhering to the surface.

At higher magnifications the nature of the particle surface is more clearly illustrated (Fig. 16). Figure 16(a), shows submicron-sized spheres (microparticles) tightly bound together in clusters. Submicron pores are apparent within the small clusters, but much larger pores on the order of 2–5 μm are visible as well. The hierarchical structure is consistent with that reported by Kakugo et al.[10,11] and Vermel et al.[13]

The addition of copolymer changes the nature of the particle morphology. At modest levels of copolymer content ($\sim$ 15 wt %), the elastomeric phase simply fills in the small voids among the microparticles, while the 2–5 μm pores are retained. At 40 wt % the elastomer has filled the small pores and some of the medium-sized pores. The presence of the elastomer as "pools" of nontextured material is clearly observable. At 70 wt % the elastomeric phase does not form pools but has engulfed the homopolymer in much the same way a sticky sap or melted plastic might cover adjacent material. It is very interesting, in light of this apparent flowability, that large pores still remain at the surface of the polymer particle.

Also observable are differences in the surface morphology of the impact copolymer particles as a function of copolymerization temperature (Fig. 17) and copolymer composition (Fig. 18) for samples with 40 wt % copolymer. Copolymerization at a low temperature leads to the formation of dis-

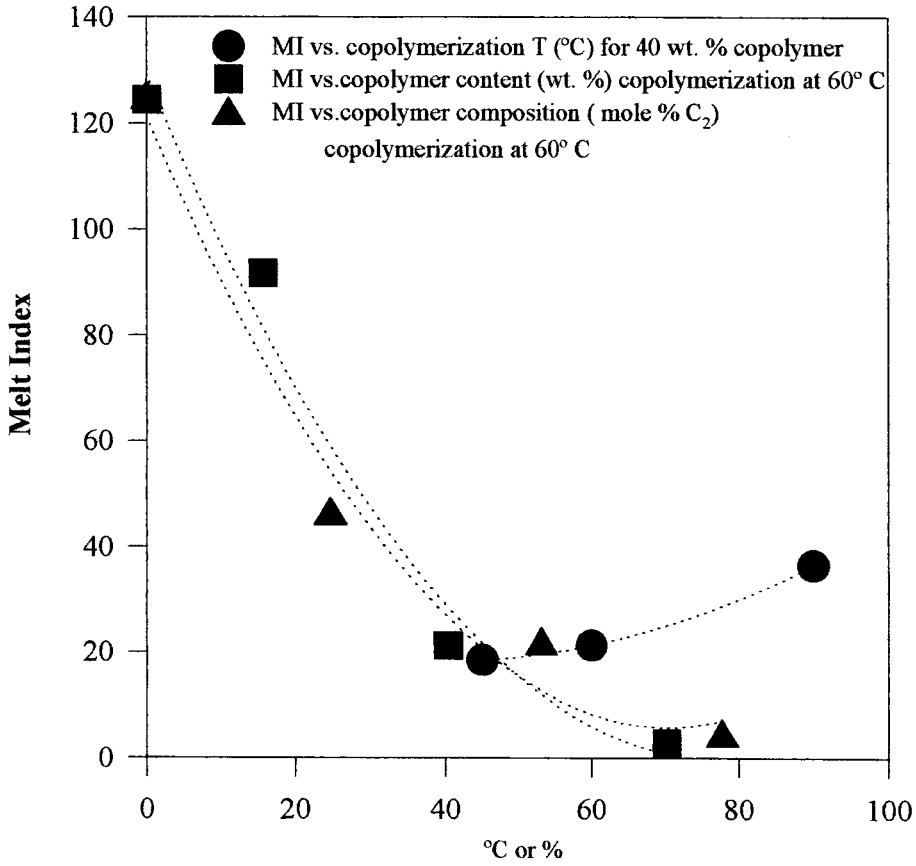

Figure 13 Melt index relationships of impact polypropylene: C_3 stage at 70°C, 3.1 atm, 5 mol % H_2; C_2/C_3 copolymerization at 1.7 atm, 5 mol % H_2.

tinct elastomeric domains in the material (although they do not appear to have "pooled" or to seem liquidlike), while at 90°C the copolymer appears to have flowed and fused the polymer together. Under identical polymerization conditions, particles with 40 wt % copolymer but with different copolymer composition have differing morphologies. The product with ~ 25 mol % ethylene in the copolymer phase resembles propylene homopolymer, and the product with ~ 80 mol % ethylene in the copolymer is crumbly in texture and closer to that observed for the polyethylene homopolymer.[26] A two-phase heterophasic structure is present at intermediate compositions, in which the copolymer has a significant amorphous content.

Sections of embedded particles (Fig. 19) reveal the presence of large pores, holes, or channels deep within both the homopolymer and copolymer particles. Note that the particle with 70 wt % copolymer is actually hollow, and no embedding resin was able to penetrate into the interior of this particle, suggesting that pores near the outer layers of the particle were choked shut with copolymer. TEM analysis of a 675-nm slice of sample containing 15 wt % copolymer shows the presence of small catalyst primary particles within submicron-sized polypropylene microparticles surrounded by a thin film of copolymer (Fig. 20).

Scanning FTIR, with an IR beam width of 16 μm, was used to test for composition gradients across the radius of impact for copolymer particles ranging from 15% to 70% copolymer content and are shown in Figure 21. No gradients were observed for the three copolymer contents, and there was excellent agreement with the ethylene content calculated from the reactor mass balance. The small rise in ethylene content close to the surface of the 70 wt % particle may result from a layer of copolymer on the surface of the particle.

Powder Morphology

The particle size distribution of the impact polypropylene samples is quite broad and reflects that of the catalyst (Fig. 22). Better replication of

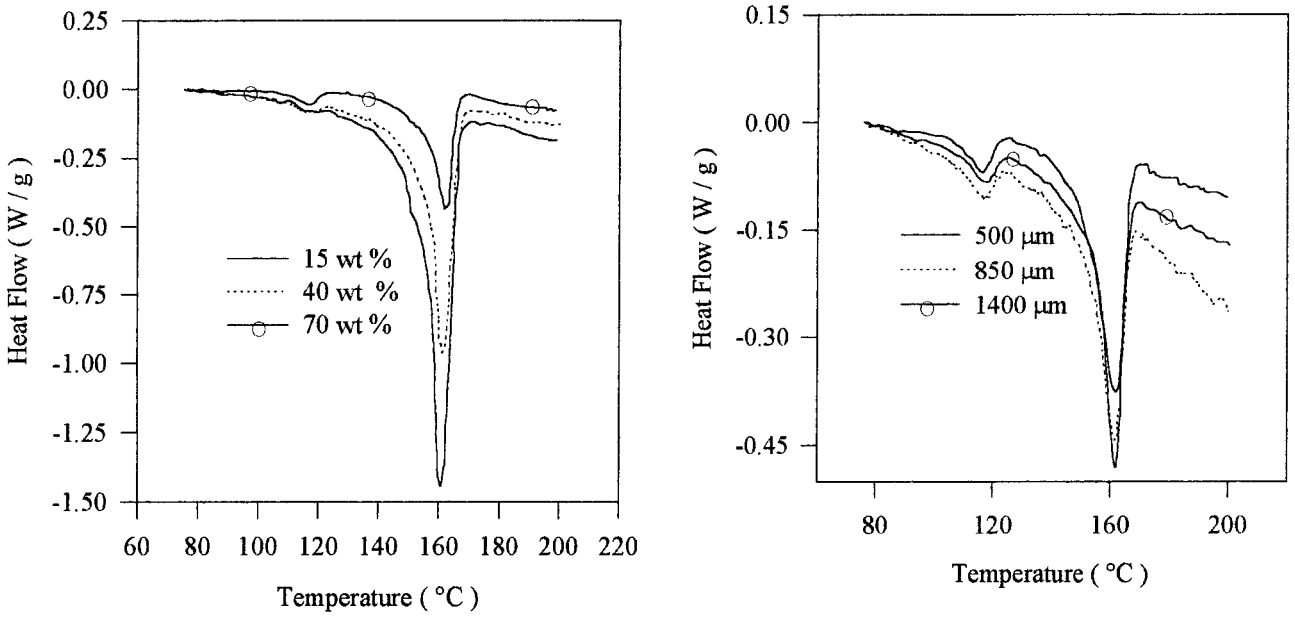

Figure 14 DSC endotherms for impact polypropylene—(a) for various copolymer contents, (b) for various particle sizes (70 wt % copolymer); C_3 stage at 70°C, 3.1 atm, 5 mol % H_2; C_2/C_3 copolymerization at 1.7 atm, 5 mol % H_2, 60 mol % C_3.

the original catalyst size distribution was obtained with homopolymer. The presence of copolymer on the particle surfaces leads to sticking and broadening of the particle size distribution, making mechanical sieving difficult for high copolymer content samples.

Mercury intrusion porosimetry results performed on the products are difficult to assess with confidence. Porosimetry results (not shown) combined with SEM analysis do indicate, however, that all the samples prepared over a range of experimental conditions retain some level of porosity, albeit, at a low level.

As evident in Figure 23, the bulk density of the powder declines significantly as copolymer content increases. A flowability test (ASTM D-1895-89, not shown here) indicated that samples with 40 wt % copolymer and higher could not flow in the test apparatus because of particle sticking. Sticking is clearly a major cause of bulk density deterioration and flowability problems.

Photographs of the polymer powder taken from a 1 mm sieve tray after separation from the Teflon™ seed bed and subsequent drying are shown in Figure 24. Good quality spherical particles are produced in the reactor; however, as the copolymer content increases, particle sticking becomes more serious.

RESULTS AND DISCUSSION

This work has studied the development of impact polypropylene produced with a $TiCl_4/MgCl_2$ catalyst over a range of operating conditions in gas phase. Newly developed experimental equipment has permitted a better understanding of the catalyst kinetics and the morphological growth of the granules.

The catalyst system used in this study is extremely complex. No doubt much of this is because of the presence of multiple site types, as substantiated by the broad molecular weight distributions and kinetic rate profiles. The different sites may be related to the different oxidation states of the Ti atom (say, Ti^{+3} and Ti^{+2}), and their initial distribution is most likely related to catalyst preparation conditions such as cocatalyst/catalyst ratio and contacting time. Decay of the sites and transformations between the two are probable as indicated by the instantaneous polymerization rate profiles.

In this work the catalyst was found to be immediately active for ethylene or propylene homopolymerization. Evidence for slow activation of the catalyst by ethylene as reported by others was not found.[1,22,23,27] During copolymerization, however, the presence of both monomers led to activation of the catalyst. The comonomer rate en-

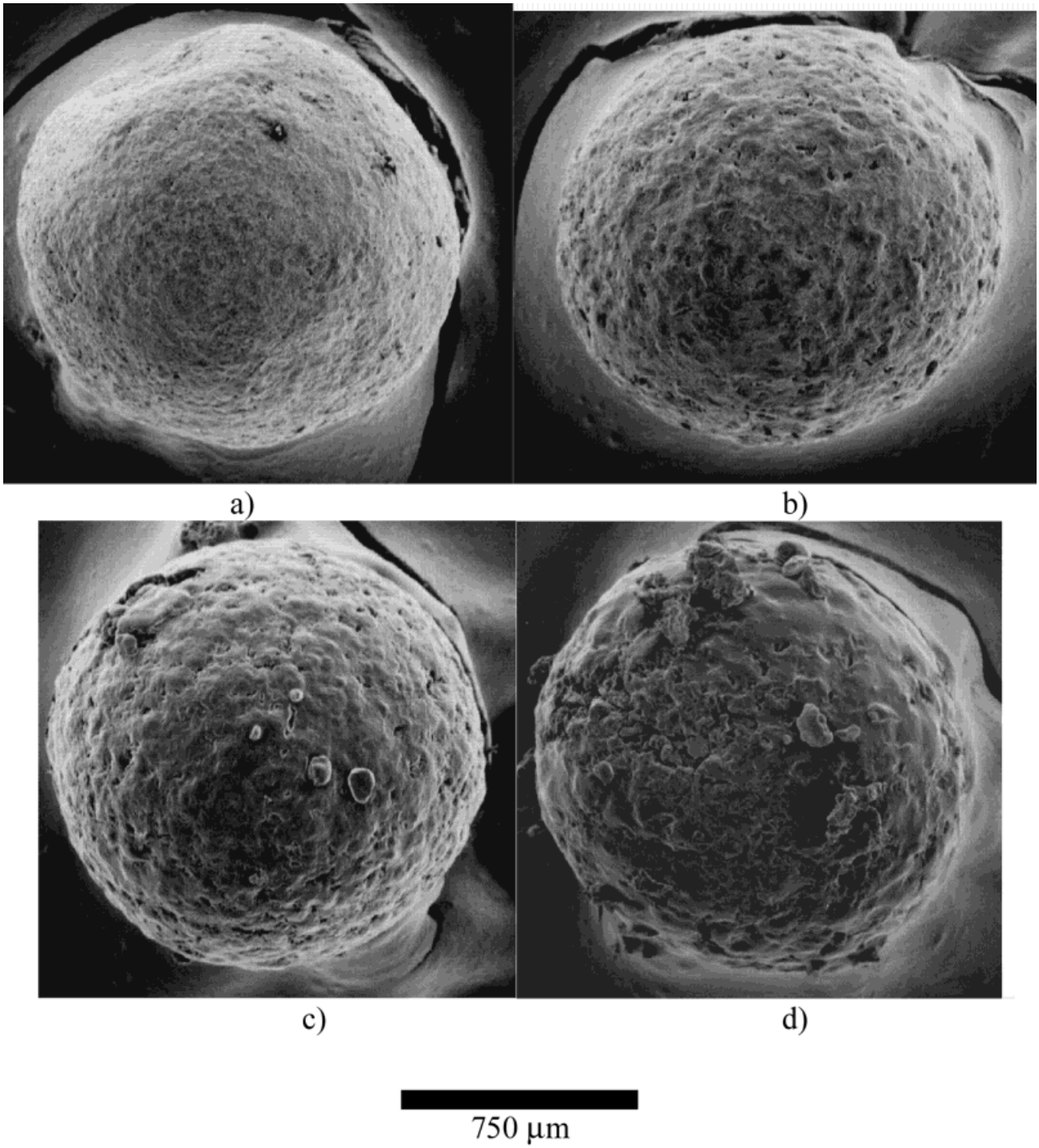

Figure 15 Surface SEM descriptions of impact copolymer at 40× magnification—(a) homopolymer, (b) 15 wt % copolymer, (c) 40 wt % copolymer, (d) 70 wt % copolymer; C_3 stage at 70°C, 3.1 atm, 5 mol % H_2; C_2/C_3 copolymerization at 1.7 atm, 5 mol % H_2, 60 mol % C_3.

hancement effect is a common feature to both Metallocene and Ziegler–Natta catalysts. The work of Calabro and Lo using ethylene and hexene indicates that the comonomer rate enhancement effect is most pronounced early in the reaction and that the rate enhancement effect de-

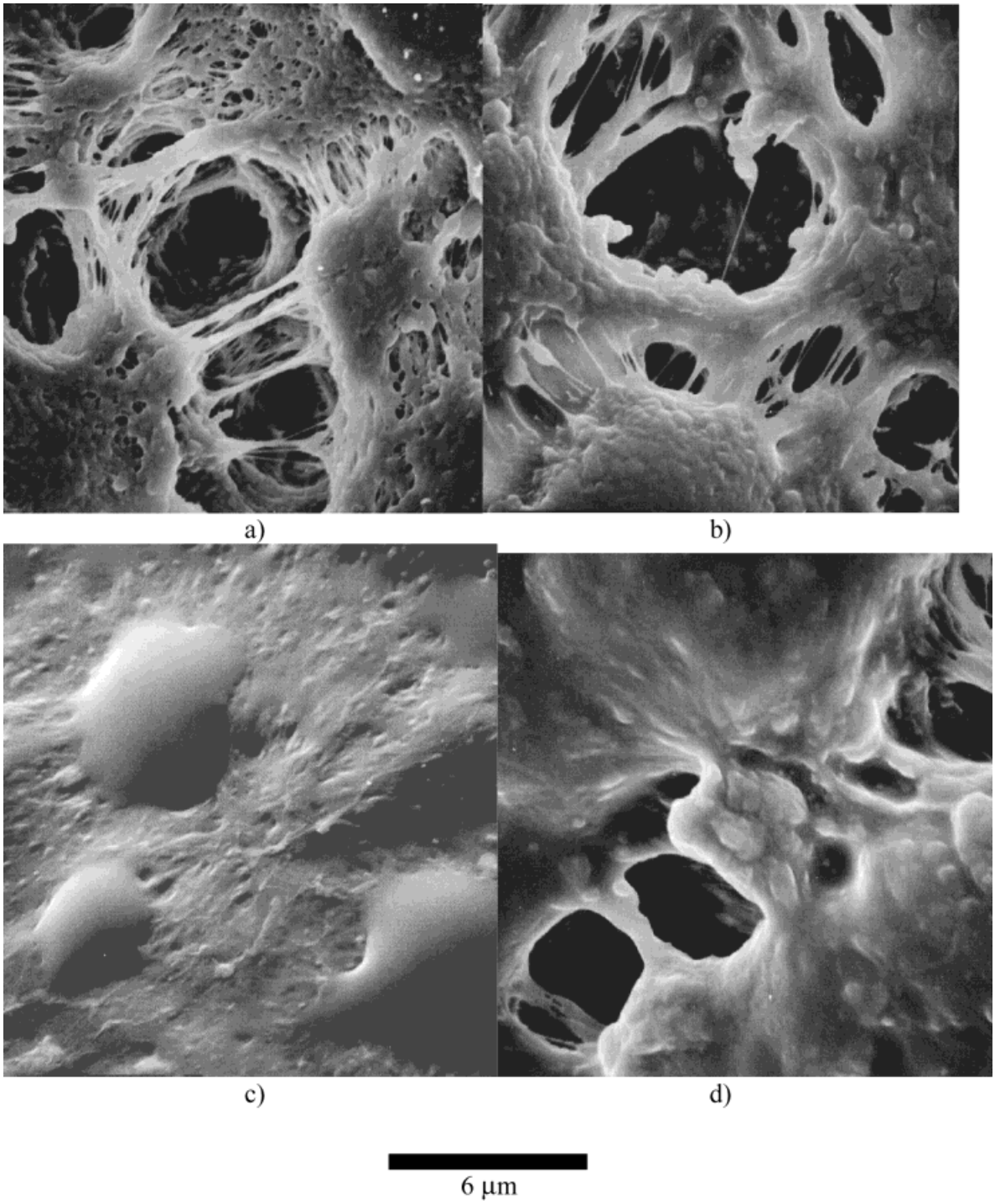

Figure 16 Surface SEM descriptions of impact copolymer at 5000× magnification for (a) homopolymer, (b) 15 wt % copolymer, (c) 40 wt % copolymer, (d) 70 wt % copolymer; C_3 stage at 70°C, 3.1 atm, 5 mol % H_2; C_2/C_3 copolymerization at 1.7 atm, 5 mol % H_2, 60 mol % C_3.

creases with time.[27] If the addition of comonomer is sufficiently delayed, no rate enhancement is observed. Activation of the catalyst by comonomer was proposed to explain these results. Tait et al.[28] found that rate enhancement of ethylene occurs when the catalyst is prepolymerized with pro-

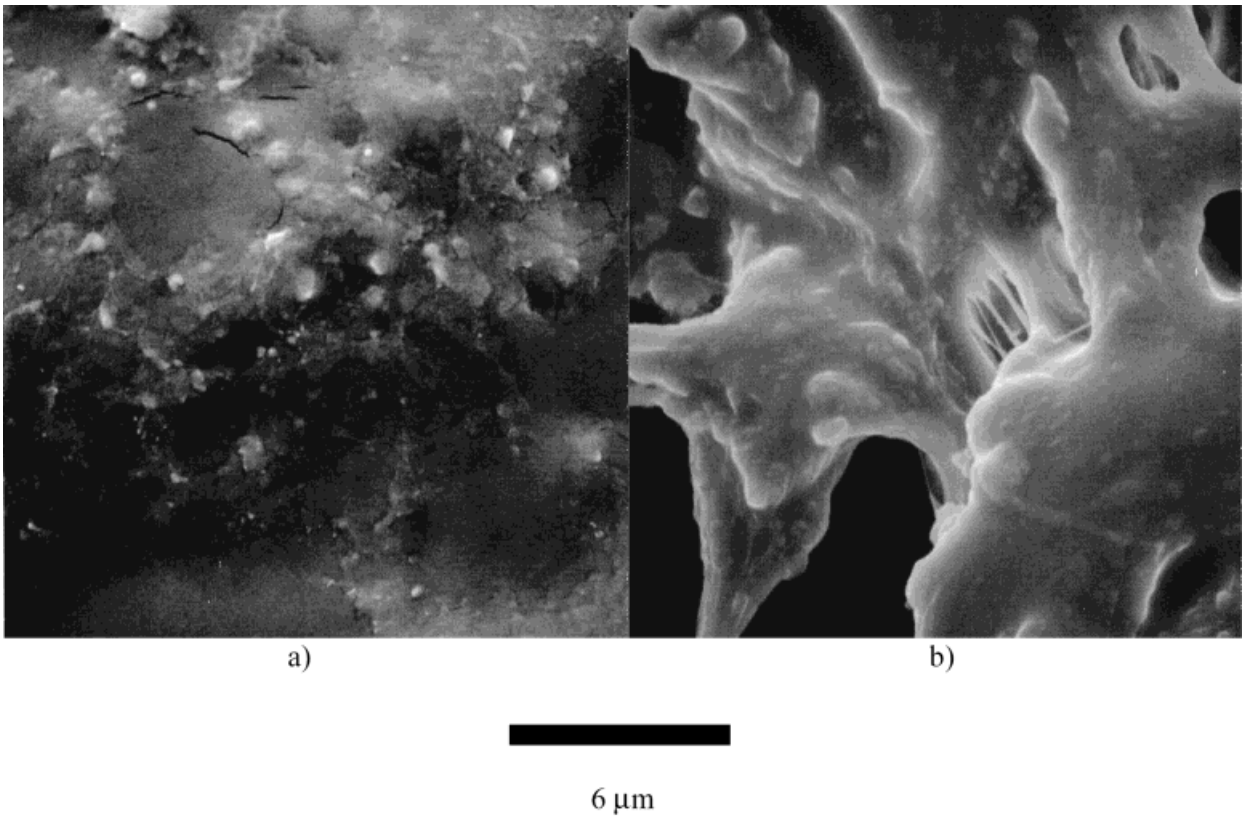

Figure 17 Surface SEM as a function of copolymerization temperature—a) 45°C, b) 90°C; C_3 stage at 70°C, 3.1 atm, 5 mol % H_2; C_2/C_3 copolymerization at 1.7 atm, 5 mol % H_2, 60 mol % C_3.

pylene, even after propylene is removed. They hypothesized that there was an increase in the number of propagation centers. Similar effects have been found with gas-phase polymerization with an unsupported $TiCl_3$ catalyst.[1] Chen also found that feeding ethylene after propylene homopolymerization leads to decreased propylene reactivity.[1] Larger rate enhancement effects were noted as the prepolymerization time increased. In this work, however, the "activation," or slow enhancement, of the catalyst rate in the presence of ethylene and propylene did not appear to be time dependent.

The results of this work are consistent with the and trigger models previously proposed by others. Karol et al.[29] have suggested that the catalyst site consists of two vacant coordinating positions in which the monomers act as Lewis bases or coordinating ligands and can influence the catalyst polymerization behavior. We assume that the titanium on the catalyst exists principally in two oxidation states, Ti^{+3} and Ti^{+2}, and both are active for polymerization. However, the monomers must first coordinate with the catalyst to activate it. We denote the different sites with a superscript ^{e} (e = ethylene) or ^{p} (p = propylene) to represent the coordinating ligand attached to the site. Thus, four principal sites can be formed and are denoted by Ti^{+3p}, Ti^{+3e}, Ti^{+2p}, Ti^{+2e}. Since the catalyst is immediately active for polymerization, we assume that this reaction is very fast for both ethylene and propylene. It is assumed that Ti^{+3} is more reactive when the propylene molecule is used as the ligand, as compared to when ethylene is used (i.e., $Ti^{+3p} > Ti^{+3e}$). The Ti^{+3} site is modeled as a fast deactivating site, while the Ti^{+2} is more stable but less active for homopolymerization of both monomers. In the presence of ethylene and propylene it is proposed that there is a competitive coordination by both monomers on the various sites. Furthermore, to explain the apparent "activation" of the catalyst observed in this work, we suggest the coordination of both ethylene and propylene together at the Ti^{+2} site leads to the formation of another highly or "super"-active site, denoted by Ti^{+2s}.

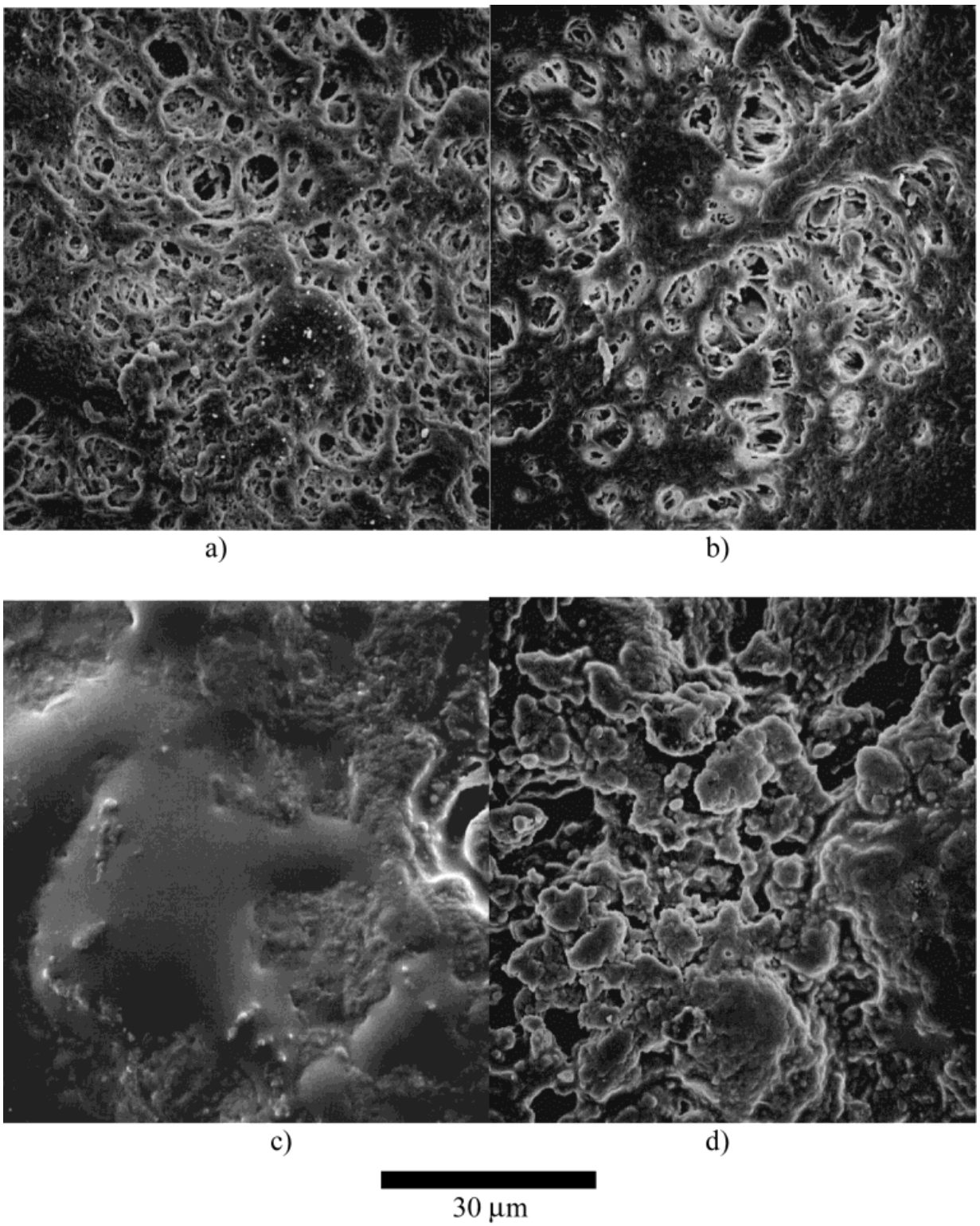

Figure 18 Surface SEM as a function of copolymer ethylene composition (40 wt % copolymer)—(a) homopolymer; (b) 24.7 mol % C_2; (c) 50 mol % C_2; (d) 77.8 mol % C_2. C_3 stage at 70°C, 3.1 atm, 5 mol % H_2; C_2/C_3 stage at 1.7 atm, 5 mol % H_2, 60 mol % C_3.

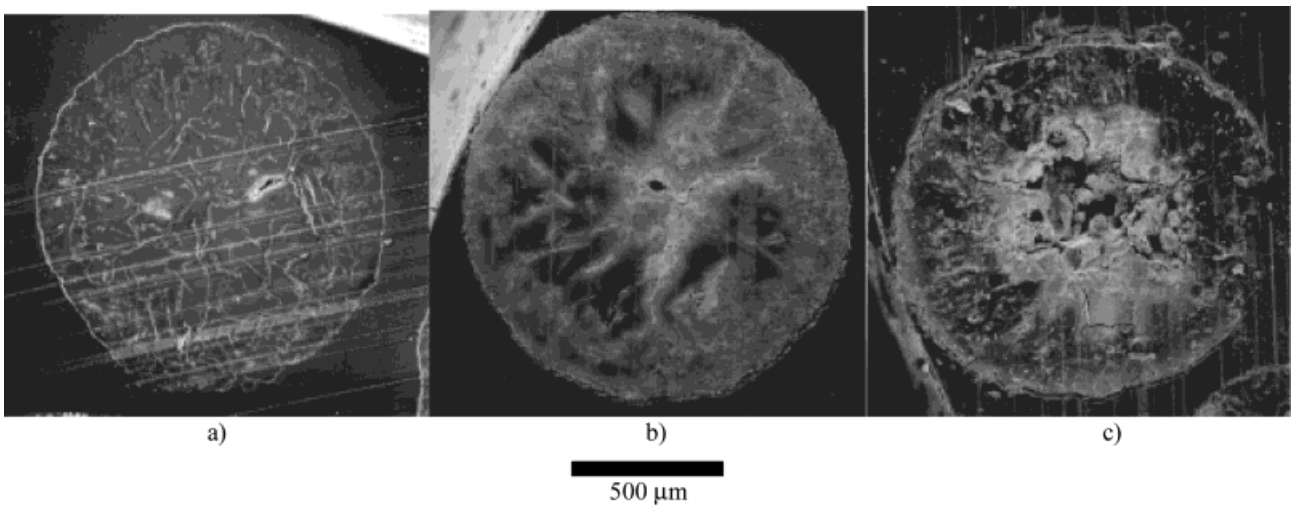

Figure 19 Sectioned SEMs of impact copolymer at 60× magnification—(a) 15 wt % copolymer, (b) 40 wt % copolymer, (c) 70 wt % copolymer: C_3 stage at 70°C, 3.1 atm, 5 mol % H_2; C_2/C_3 copolymerization at 1.7 atm, 5 mol % H_2, 60 mol % C_3.

The ability of hydrogen to affect propylene rate has been reported by Guastalla and Giannini.[30] Their work indicates initial propylene rate can be boosted by a factor of 2.5 as hydrogen partial pressure is increased. Yuan et al.,[31] Choi and Ray,[32] and Spitz et al.[24] have found that although hydrogen at low concentrations causes a rate increase, higher hydrogen levels lower activity and increase deactivation. The effect of hydrogen addition on propylene polymerization was found to be reversible, and no effect on ethylene rate was noted. Copolymerization experiments with ethylene showed that hydrogen caused a rate boost, but the boost was not as significant as when propylene homopolymerization was conducted. Hamba et al.,[22,23] on the other hand, have found hydrogen reduces ethylene rate for a supported $TiCl_4$–$MgCl_2$ catalyst without the use of an external donor (Fig. 25).

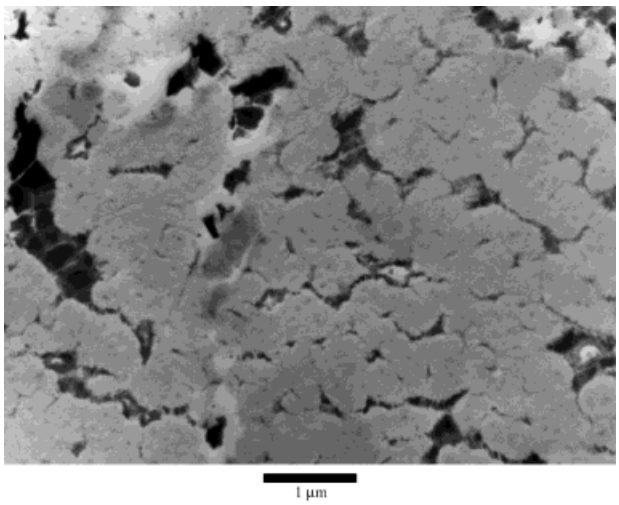

Figure 20 TEM of 15 wt % copolymer: C_3 stage at 70°C, 3.1 atm, 5 mol % H_2; C_2/C_3 copolymerization at 1.7 atm, 5 mol % H_2, 60 mol % C_3.

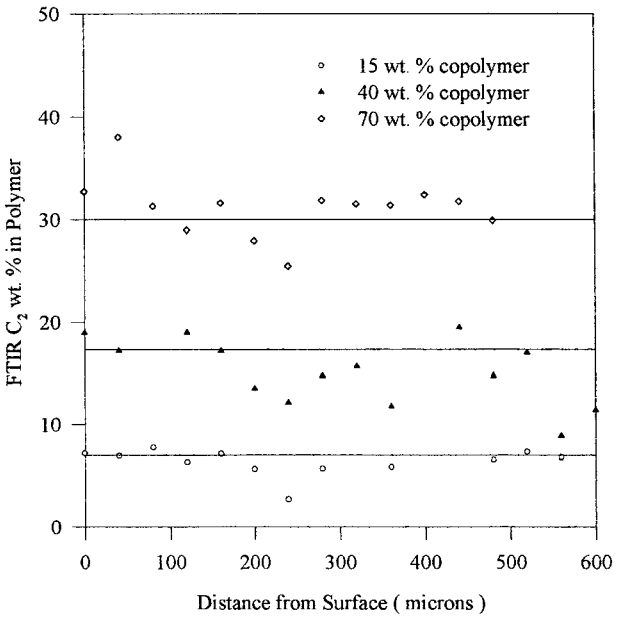

Figure 21 Scanning FTIR results (lines represent theoretical value from reactor mass balance): C_3 stage at 70°C, 3.1 atm, 5 mol % H_2; C_2/C_3 copolymerization at 1.7 atm, 5 mol % H_2, 60 mol % C_3.

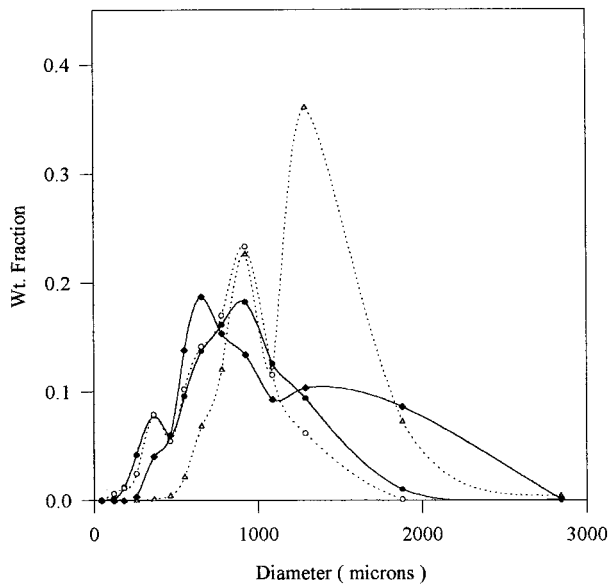

Figure 22 Particle size distribution of impact copolymer.

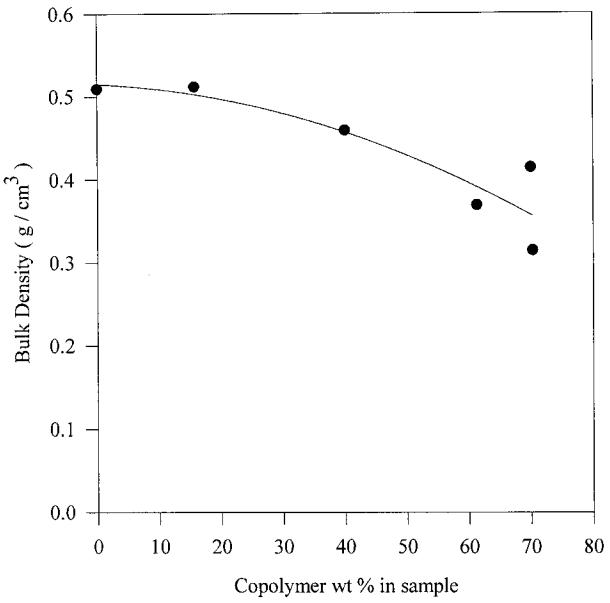

Figure 23 Bulk density of impact polypropylene as a function of copolymer content: C_3 stage at 70°C, 3.1 atm, 5 mol % H_2; C_2/C_3 copolymerization at 1.7 atm, 5 mol % H_2, 60 mol % C_3.

Many theories have been proposed to describe the effect of hydrogen on polymerization, including an increase in active sites,[33] changes in the propagation rate constant,[34] and changes in the oxidation state.[22,23] The experimental data in this work is consistent with the theory of "site cleaning" by hydrogen, indicated by Busico et al. and

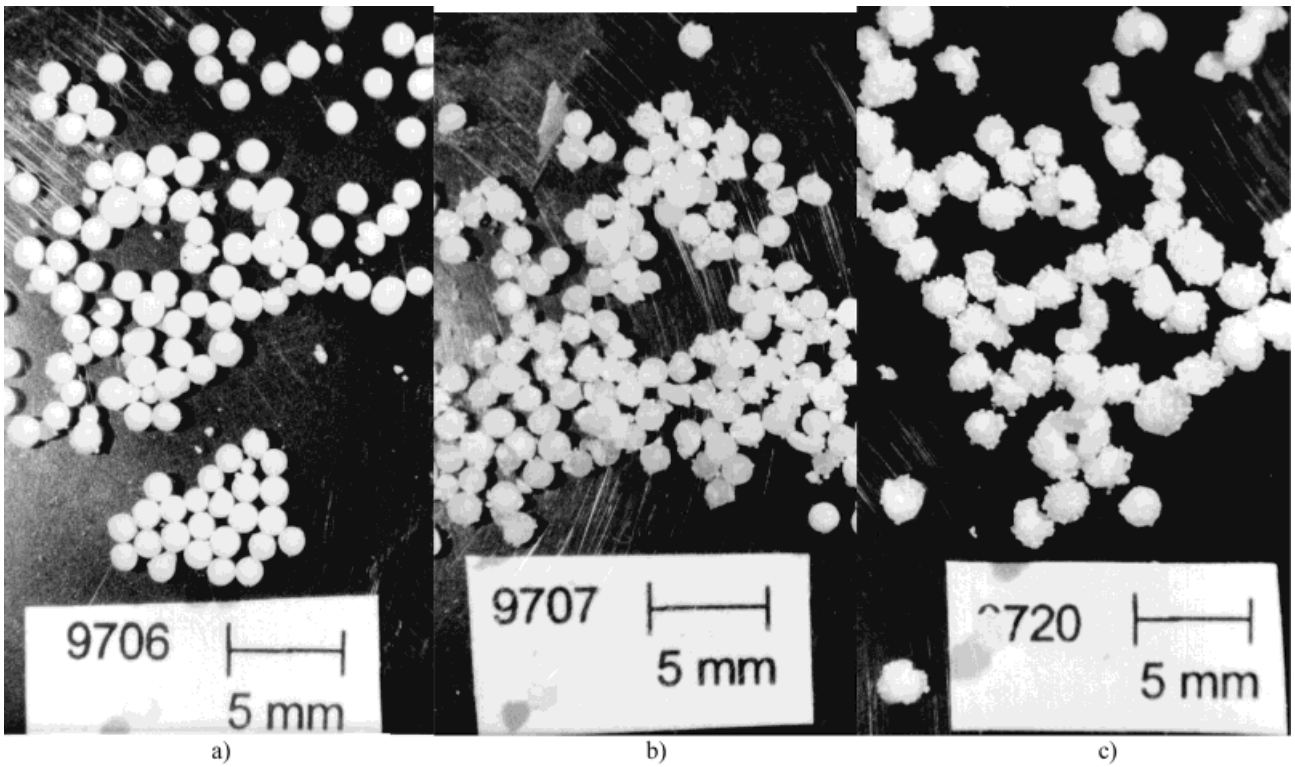

Figure 24 Photo of impact polypropylene particles.

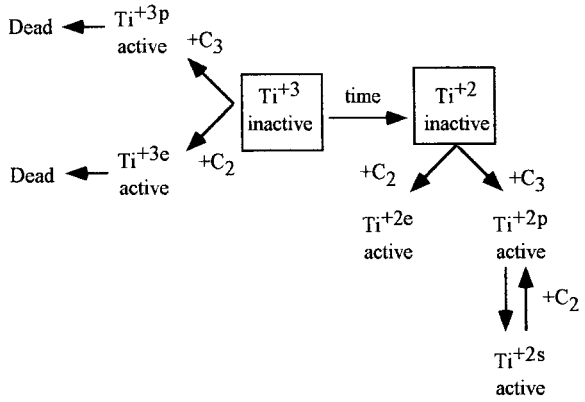

Figure 25 Proposed kinetic model ($TiCl_4/MgCl_2$ catalyst) for ethylene and propylene polymerization.

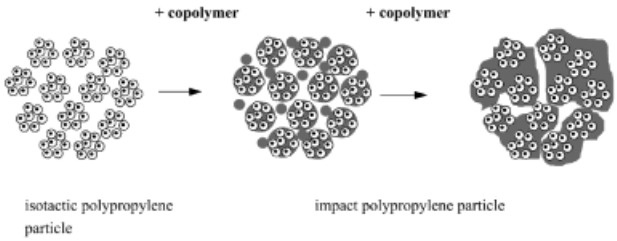

Figure 26 Proposed model of impact polypropylene particle growth.

Tsutsui et al., in which chain transfer to hydrogen removes a slow polymerizing propylene molecule inserted in the tail-to-tail position at the catalyst site.[35,36] Thus, hydrogen only affects the rate of propylene self-propagation. The insertion of hydrogen during site cleaning may increase the deactivation rate of the catalyst.

From this work a reasonable picture of the particle growth of impact polypropylene granules has been obtained. During the homopolymerization stage, catalyst fragments are surrounded by a layer of polypropylene and evolve into submicron-sized "microparticles." Although each microparticle grows independently, their clustering to form larger structures is common. The resulting granule contains both submicron-sized pores separating the microparticles and larger micron-sized ones that separate the clusters. Total porosity in the granule is fairly low, but some porosity always remains in the particle.

The copolymer phase does not remain encapsulated within the polypropylene microparticles but progressively expands into the small micropores, then into larger macropores. Yet, during this process large pores, macro cracks, and long voids deep in the polymer particle remain, resulting in total porosities similar to that of the homopolymer. The observed morphology of the impact polypropylene granules in turn is dependent on the nature of the copolymer phase. We have shown that an amorphous copolymer phase can be made to form pools of segregated rubbery domains, flow into a continuous "gluing" phase or simply set in the particle pores. Affected by this process are conditions that favor low copolymer viscosity and high mobility, such as high reaction temperature, low polymer crystallinity, and low

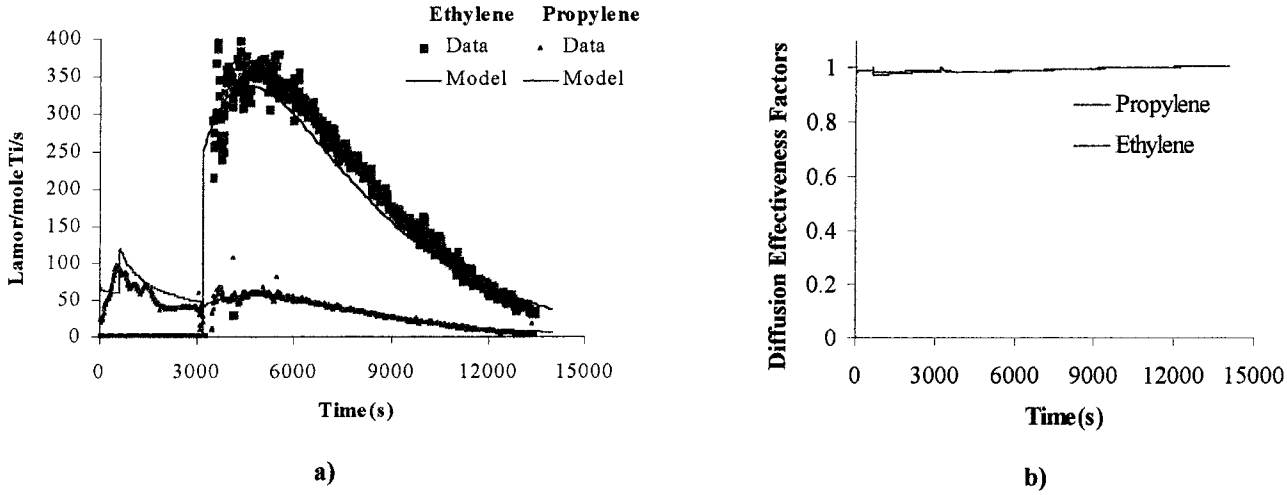

Figure 27 Comparison of model simulations (lines) with experimental data (points): (a) rate versus time, (b) efficiency factor: C_3 stage at 70°C, 3.1 atm: C_2/C_3 stage at 60°C, 3.1 atm, 5% H_2, 60 mol % C_3.

Table III Simulation Parameters

Properties	Value	
Catalyst diameter	74 μm	
Initial catalyst porosity	0.5	
Minimum porosity	0.10	
Particle relative velocity	2 cm/s	
Heat transfer correlation	Ranz Marshall	
Mass transfer correlation	Ranz Marshall	
Fluid fraction in reactor	0.6	
Properties	**Value @ 70°C**	**Activation Energy**
Maximum potential sites	1	
Initial fraction of site 1	0.298	
Initial fraction of site 2	0.702	
Site transformation by species		
Site 2 + $C_2 \rightarrow$ Site 4	0.02 L/mol Ti/s	18.47 Kcal/mol Ti/s
Site 1 + $C_2 \rightarrow$ Site 3	0.3 L/mol Ti/s	18.47 Kcal/mol Ti/s
Site 2 + $C_2 \rightarrow$ Site 3	0.03 L/mol Ti/s	18.47 Kcal/mol Ti/s
Site 1 Spontaneous deactivation	0.0008 s^{-1}	18.47 Kcal/mol Ti/s
Site 2 Spontaneous deactivation	3.5×10^{-5} s^{-1}	18.47 Kcal/mol Ti/s
Site 3 Spontaneous deactivation	3×10^{-4} s^{-1}	18.47 Kcal/mol Ti/s
Site 1 Site deactivation by H_2	0.03 L/mol Ti/s	18.47 Kcal/mol Ti/s
Site 2 Site deactivation by H_2	0.005 L/mol Ti/s	18.47 Kcal/mol Ti/s
Site 3 Site deactivation by H_2	0.02 L/mol Ti/s	18.47 Kcal/mol Ti/s
Site 1 Propagation		
* of C_3 on chain ending with C_3	155 L/mol Ti/s	9.9 Kcal/mol Ti/s
* of C_3 on chain ending with C_2	283 L/mol Ti/s	9.9 Kcal/mol Ti/s
* of C_2 on chain ending with C_3	1174 L/mol Ti/s	9.9 Kcal/mol Ti/s
* of C_2 on chain ending with C_2	1394 L/mol Ti/s	9.9 Kcal/mol Ti/s
Site 2 Propagation		
* of C_3 on chain ending with C_3	103 L/mol Ti/s	9.9 Kcal/mol Ti/s
* of C_3 on chain ending with C_2	189 L/mol Ti/s	9.9 Kcal/mol Ti/s
* of C_2 on chain ending with C_3	783 L/mol Ti/s	9.9 Kcal/mol Ti/s
* of C_2 on chain ending with C_2	930 L/mol Ti/s	9.9 Kcal/mol Ti/s
Site 3 Propagation		
* of C_3 on chain ending with C_3	289 L/mol Ti/s	9.9 Kcal/mol Ti/s
* of C_3 on chain ending with C_2	530 L/mol Ti/s	9.9 Kcal/mol Ti/s
* of C_2 on chain ending with C_3	2191 L/mol Ti/s	9.9 Kcal/mol Ti/s
* of C_2 on chain ending with C_2	2603 L/mol Ti/s	9.9 Kcal/mol Ti/s
Site 4 Propagation		
* of C_3 on chain ending with C_3	103 L/mol Ti/s	9.9 Kcal/mol Ti/s
* of C_3 on chain ending with C_2	189 L/mol Ti/s	9.9 Kcal/mol Ti/s
* of C_2 on chain ending with C_3	783 L/mol Ti/s	9.9 Kcal/mol Ti/s
* of C_2 on chain ending with C_2	930 L/mol Ti/s	9.9 Kcal/mol Ti/s

polymer molecular weights. The granules containing crystalline copolymers closely resemble the morphologies of homopolymer produced from the principle comonomer. A proposed model is summarized in Figure 26.

Under the conditions studied in this work, monomer diffusion limitations were not detected. Computer simulations (Fig. 27) using a model of particle growth developed previously and kinetic parameters summarized in Table III agree with these experimental observations.[37] Although the porosity of the granule is low, the macropores, large cracks, and channels are sufficient to permit adequate transport of monomer to the interior of

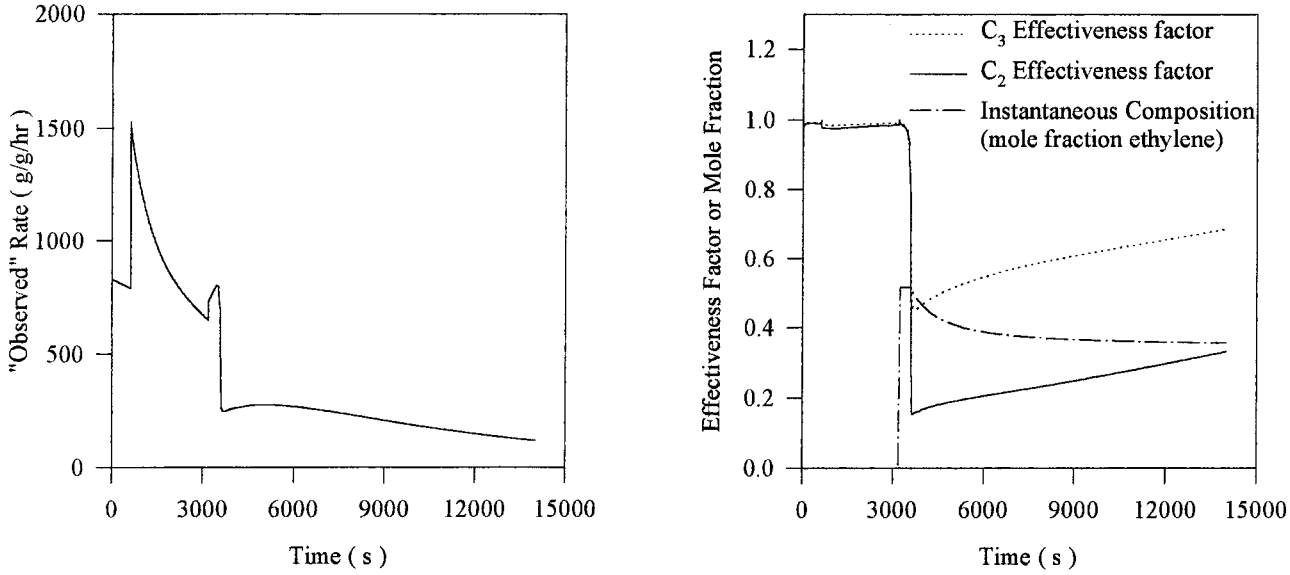

Figure 28 Model predictions for particles with complete pore filling—(a) rate versus time, (b) efficiency factor and composition: C_3 stage at 70°C, 3.1 atm; C_2/C_3 stage at 60°C, 3.1 atm, 5% H_2, 60 mol % C_3.

the granule for gas-phase polymerization. Furthermore, simulations at industrial reaction conditions (not shown) indicate that monomer mass transport would be still sufficient to avoid diffusional limitations. This assumes of course that the particle morphology formed under high monomer concentration and high production rate is similar to that observed under the less severe conditions used in this work. Our conclusions are based on work with a specific catalyst within a range of experimental conditions using a consistent procedure for catalyst activation and prepolymerization. Generalization of these conclusions to other systems such as metallocenes may not be possible.

Our results clearly show that if the pores of the particle are completely occluded with copolymer, the monomer will be forced to diffuse through polymer only; in this situation diffusion limitations would be very noticeable even under the mild experimental conditions of this work (Fig. 28). Ethylene would be more diffusion limited than propylene, and the composition and crystallinity of copolymer would change over the course of the polymerization. Clearly the preservation of some porosity in the impact polypropylene granule, such as macro cracks in the particle or small well-connected channels, is essential for maintaining adequate diffusion of monomer and is quite possibly a catalyst design target.

The presence of a segregated copolymer phase ultimately leads to sticky copolymer on the surface of the particle that has been shown to be responsible for particle sticking and poor bulk density. As indicated by Kakugo et al.,[16] sticky copolymer granules require higher fluidization velocities and are difficult to handle in a commercial process. Protecting the surface of the particle by proper design of the catalyst morphology[8] or selectively poisoning the catalyst sites on the granule surface to prevent copolymerization are possible methods of addressing particle sticking. In our experiments with the small stirred-bed reactor, however, particle sticking was not serious enough to stop the polymerization experiments, even at 70 wt % copolymer.

The authors are indebted to the National Science Foundation, the Industrial Sponsors of the University of Wisconsin Polymerization Reaction Engineering Laboratory (UWPREL) for their financial support of this research. Special thanks to Drs. Rich Fezza and Mike Wolkowicz at Montell Polyolefins for coordinating the particle microscopy, SEM, and scanning FTIR work for the impact polypropylene samples. Thanks also to Drs. Shiaw Ju, Simon Zhang, and Charles Cozewith at Exxon Chemicals for providing the DSC, MI/MFR, mercury porosimetry, and GPC work.

M_n number-average molecular weight
M_w weight-average molecular weight

r_1, r_2 copolymerization reactivity ratios 1 = C_3, 2 = C_2
ε_p particle void fraction
φ_i weight fraction polymer phase i

REFERENCES

1. Chen, C. Ph.D. Thesis, University of Wisconsin–Madison, 1993.
2. Hutchinson, R. A. Ph.D. Thesis, University of Wisconsin–Madison, 1990.
3. Rincon-Rubio, L. M.; Wilen, C. E.; Lindfors, L. E. Eur Polym J 1990, 26(2), 171.
4. Rotzinger, B. Ph.D. Thesis, Eidgenossischen Technischen Hochschule-Zurich, 1984.
5. Tait, P.; Jaber, I.; Loontjens, A. Catalytic Olefin Polymerization; In Proc Intl Symp Recent Dev Olefin Polym Catalysts, Tokyo, Oct. 23–25, Keii, T., Soga, K., Eds.; Elsevier: Amsterdam, 1990.
6. Bukatov, G. D.; Zaikovskii, V. I.; Zakharov, V. A.; Kryukova, G. N.; Fenelonov, V. B.; Zagrafskaya, R. V. Polym Sci U.S.S.R. 1982, 23(3), 599.
7. Ferrero, M.; Sommer, R.; Spanne, P.; Jones, K. W.; Conner, W. C. J Polym Sci 1993, 31, 2507.
8. Galli, P.; Haylock, J. Prog Polym Sci 1991, 16, 443.
9. Hock, C. J Polym Sci: Part A-1 1966, 4, 3055.
10. Kakugo, M.; Sadatoshi, H.; Yokoyama, M.; Kojima, K. Macromolecules 1989, 22, 547.
11. Kakugo, M.; Sadatoshi, H.; Sakai, J.; Yokoyama, M. Macromolecules 1989, 22, 3172.
12. Noristi, L.; Marchetti, E.; Baruzzi, G.; Sgarzi, P. J Polym Sci: Polym Chem Ed 1994, 32, 3047.
13. Vermel, E.; Zakharov, V.; Fenelonov, V.; Zaikovskii, V.; Zagrafskaya, R.; Moroz, E.; Bukatov, G. Kinetika i Kataliz 1981, 22(2), 480.
14. Wristers, J. J Polym Sci: Polym Physics Ed 1973, 11, 1601.
15. Wristers, J. J Polym Sci: Polym Physics Ed 1973, 11, 1619.
16. Kakugo, M.; Hashimoto, M.; Isobata, J. Presented at the 1987 AIChE Annual Meeting, New York, 1987.
17. Kakugo, M.; Sadatoshi, H.; Sakai, J. In Catalytic Olefin Polymerization; Keii, T., Soga, K., Eds.; Elsevier: New York, 1990; p 345.
18. Simonazzi, T.; Cecchin, G.; Mazzullo, S. Prog Polym Sci 1991, 16, 303.
19. Galli, P. Presented at the 6th International Workshop on Polymer Reaction Engineering, Berlin, 1998.
20. Hoel, E. L.; Cozewith, C.; Byrne, G. D. AIChE Journal 1994, 40(10), 1669.
21. Debling, J. A. Ph.D. Thesis, University of Wisconsin-Madison, 1997.
22. Hamba, M.; Han-Adebekun, G. C.; Ray, W. H. J Polym Sci Part A: Polym Chem 1997, 35, 2075.
23. Han-Adebekun, G. C.; Hamba, M.; Ray, W. H. J Polym Sci, Part A: Polym Chem 1997, 35, 2063.
24. Spitz, R.; Masson, P.; Bobichon, C.; Guyot, A. Makromolekulare Chemie 1989, 190, 717.
25. Brandrup, J.; Immergut, E. H. Polymer handbook; Wiley: New York, 1989.
26. Kim, I.; Woo, S. I. Polymer J 1989, 21(9), 697.
27. Calabro, D. C.; Lo, F. Y. In Transition Metal Catalyzed Polymerizations Ziegler–Natta and Metathesis Polymerizations; Quirk, R. P., Ed.; Cambridge Univ. Press: Cambridge, UK, 1988; p. 729.
28. Tait, P.; Berry, I.; Abozeld, A. Presented at 6 seminario brasileiro de catalise; Salvador-BA, 1991.
29. Karol, F. J.; Kao, S. C.; Cann, K. J. J Polym Sci: Part A: Polym Chem 1993, 31, 2541.
30. Guastalla, G.; Giannini, U. Makromolekulare Chemie, Rapid Communications 1983, 4, 519.
31. Yuan, H.-G.; Taylor, T. W.; Choi, K. Y.; Ray, W. H. J Appl Polym Sci 1982, 27, 1691.
32. Choi, K. Y.; Ray, W. H. J Appl Polym Sci 1985, 30, 1065.
33. Parsons, I. W.; Al Turki, T. M. Polymer Comm 1988, 30, 720.
34. Kioka, M.; Kashiwa, N. J Mackromolecular Sci Chem 1991, A28, 865.
35. Busico, V.; Cipullo, R.; Corradini, P. Makromolekulare Chemie, Rapid Communications 1992, 13, 15.
36. Tsutsui, T.; Kashiwa, N.; Mizuno, A. Makromolekulare Chemie, Rapid Communications 1990, 11, 565.
37. Debling, J. A.; Ray, W. H. Ind Eng Chem Res 1995, 34(10), 3466.